INL/CON-11-21644
PREPRINT

# A Two-Dimensional Method of Manufactured Solutions Benchmark Suite Based on Variations of Larsen's Benchmark with Escalating Order of Smoothness of the Exact Solution

## M & C 2011

Sebastian Schunert
Yousry Y. Azmy

May 2011



*International Conference on Mathematics and Computational Methods Applied to Nuclear Science and Engineering (M&C 2011)*
Rio de Janeiro, RJ, Brazil, May 8-12, 2011, on CD-ROM, Latin American Section (LAS) / American Nuclear Society (ANS)
ISBN 978-85-63688-00-2

# A TWO-DIMENSIONAL METHOD OF MANUFACTURED SOLUTIONS BENCHMARK SUITE BASED ON VARIATIONS OF LARSEN'S BENCHMARK WITH ESCALATING ORDER OF SMOOTHNESS OF THE EXACT SOLUTION

**Sebastian Schunert and Yousry Y. Azmy**
Department of Nuclear Engineering
North Carolina State University
Raleigh, NC
snschune@ncsu.edu, yyazmy@ncsu.edu

## ABSTRACT

The quantification of the discretization error associated with the spatial discretization of the Discrete Ordinate(DO) equations in multidimensional Cartesian geometries is the central problem in error estimation of spatial discretization schemes for transport theory as well as computer code verification. Traditionally fine mesh solutions are employed as reference, because analytical solutions only exist in the absence of scattering. This approach, however, is inadequate when the discretization error associated with the reference solution is not small compared to the discretization error associated with the mesh under scrutiny. Typically this situation occurs if the mesh of interest is only a couple of refinement levels away from the reference solution or if the order of accuracy of the numerical method (and hence the reference as well) is lower than expected. In this work we present a Method of Manufactured Solutions (MMS) benchmark suite with variable order of smoothness of the underlying exact solution for two-dimensional Cartesian geometries which provides analytical solutions averaged over arbitrary orthogonal meshes for scattering and non-scattering media. It should be emphasized that the developed MMS benchmark suite first eliminates the aforementioned limitation of fine mesh reference solutions since it secures knowledge of the underlying true solution and second that it allows for an arbitrary order of smoothness of the underlying exact solution. The latter is of importance because even for smooth parameters and boundary conditions the DO equations can feature exact solution with limited smoothness. Moreover, the degree of smoothness is crucial for both the order of accuracy and the magnitude of the discretization error for any spatial discretization scheme.

*Key Words:* MMS, Larsen's Benchmark, Error Estimation, Code Verification.

## 1. INTRODUCTION

The accuracy of spatial discretization schemes of the Discrete Ordinate(DO) equations has been subject to extensive research both purely analytical and via numerical experiments. It is important to distinguish here between the work done in one-dimensional slab geometry on the one hand and in multi-dimensional Cartesian geometries on the other hand, because neither methods nor results can easily be extended from slab-geometry to multi-dimensional geometries. The reason for this distinction arises from two facts: First, the exact solution of the DO equations in slab geometry is infinitely often differentiable [1], while in multi-dimensional geometries

the solution exhibits limited smoothness [2]. Second, in slab geometry analytical solutions for the DO equations exist in the presence of scattering (cf. [3]) as opposed to multi-dimensional geometries, where solutions can only be obtained for purely absorbing media. The most important ramification of the first fact is that the global asymptotic rate of convergence of any spatial discretization scheme in slab geometry is an integer that solely depends on the spatial discretization scheme. This fact, along with the simplicity with which the discretized solution in any cell can be expressed in terms of the upstream cells, facilitated the determination of the global rate of convergence for a wide variety of spatial discretization schemes in slab geometry as e.g. in [4] and [5]. In multi-dimensional geometries the rate of convergence crucially depends on the smoothness of the underlying exact solution, which implies that the rate of convergence depends on the problem configuration and the specific norm applied. In general the rates of convergence is limited either by the order of the discretization scheme or the smoothness of the underlying true solution, whichever is smaller [6]. As the exact underlying solution and hence its smoothness is unknown, error estimation in multi-dimensions often resorted to numerical experiments, but this again poses the question of how to evaluate the error without knowledge of the underlying true solution. The general practice in most research done in the field is to obtain a highly accurate reference solution such that its discretization error is small compared to the discretization errors on the sequence of meshes that are used for the convergence study, cf. e.g. [6]. However, without further precaution such as an a-posteriori error estimation, the discretization error in such a "reference solution" may either be larger than assumed due to a small rate of convergence of the numerical method or the discretization error may be small but not negligible when compared with the discretization error committed on the finest meshes used in the framework of the convergence study.

Another application that demands an accurate quantification of the discretization error is computer code verification. Similar to error estimation verification usually requires the code of interest to converge to the exact solution within the framework of a mesh refinement study in order to assert correctness of the code. The general approach is to determine the theoretical rate of convergence of the spatial discretization scheme and then see whether the actual code can attain this rate of convergence. Since lack of smoothness of the underlying exact solution deteriorates the rate of convergence computer code verification usually employs test cases which possess bounded spatial derivatives up to arbitrary order. However, depending on the spatial order of the scheme bounded derivatives only up to a certain order are required; the notion of having all partial derivatives bounded just ensures this fact in the general case [7]. In this work we present a two-dimensional MMS benchmark suite for arbitrary Cartesian meshes featuring a variable degree of smoothness that addresses two of the issues mentioned above: First, it provides exact cell-averages and spatial moments of the manufactured solution thus eliminating any source of inaccuracy (within the prevailing arithmetic precision) from the reference solution. Furthermore, the variable degree of smoothness allows for a determination of the degradation of the rate of convergence in the presence of discontinuities of the exact flux or its partial derivatives. The described benchmark suite is the logical continuation of the MMS benchmark cases presented in [8] extended to arbitrary material properties, domain sizes, Cartesian grids and degrees of smoothness of the manufactured solution. In particular, [8] only treats manufactured solutions either featuring non-smooth angular fluxes or non-smooth first partial derivatives, while we develop a framework that allows an arbitrary degree to smoothness.

## 2. THE MMS REFERENCE SOLUTION

The monoenergetic DO transport equation with isotropic scattering in two-dimensional Cartesian geometry is given by:

$$\mu_n \frac{\partial \psi_n}{\partial x} + \eta_n \frac{\partial \psi_n}{\partial y} + \sigma_t \psi_n(x,y) = \sigma_s \phi(x,y) + q(x,y) \text{ if } x,y \in \mathcal{D} = (0,X) \times (0,Y) \tag{1}$$

for $n \in 1,..,N$ along with appropriate boundary conditions:

$$\psi_n(x,y) = \psi_{BC,n}(x,y) \text{ if } x,y \in \partial\mathcal{D}^- = \{x,y \in \partial\mathcal{D}, (\mu_n,\eta_n)^T \cdot \hat{n} < 0\} \tag{2}$$

and a quadrature rule to close the system of equations:

$$\phi(x,y) = \sum_{n=1}^{N} w_n \psi_n(x,y) \text{ with } \{(\mu_n,\eta_n), w_n\}_{n=1,...,N}. \tag{3}$$

In Eq. 1 $\sigma_t$ and $\sigma_s$ are the macroscopic total and scattering cross sections that we set independent of space. We denote by $\psi_n$, $\phi$ and $q$ the angular flux along direction $n$, the scalar flux and the isotropic source, respectively. Further, the rectangular spatial domain $\mathcal{D}$ is circumscribed by the boundary $\partial\mathcal{D}$ with the outward normal vector $\hat{n}$ which can be divided into the inflow boundary $\partial\mathcal{D}^-$ and the outflow boundary $\partial\mathcal{D}^+$. Boundary conditions along direction $n$ are given on the inflow boundary by $\psi_{BC,n}$. We will refer to this problem setup as the model problem. In the case of a non-scattering material, constant and equal boundary fluxes on both incoming edges and a vanishing distributed source the model problem is known as Larsen's benchmark [9]. The presented benchmark suite draws from the early work done in [9], but it allows for more freedom in the choice of the input parameters especially the boundary conditions.

The MMS formalism proceeds by choosing a solution $\psi_n(x,y)$ for $n = 1,..,N$ and then determining the source $q(x,y)$ and boundary conditions $\psi_{BC,n}$ such that the system of equations 1 through 3 is satisfied. To this end we solve Eq. 1 for $q(x,y)$:

$$q(x,y) = \mu_n \frac{\partial \psi_n}{\partial x} + \eta_n \frac{\partial \psi_n}{\partial y} + \sigma_t \psi_n(x,y) - \sigma_s \phi(x,y). \tag{4}$$

Now, for our purpose we choose the manufactured solution $\psi_n$ to be the solution of the auxiliary problem

$$\mu_n \frac{\partial \psi_n}{\partial x} + \eta_n \frac{\partial \psi_n}{\partial y} + \sigma_t \psi_n(x,y) = Q \text{ if } x,y \in \mathcal{D} = (0,X) \times (0,Y), \tag{5}$$

where $Q$ is a space independent auxiliary source to be determined later and boundary conditions for the auxiliary problem are prescribed to be the same as for the model problem. For any reasonable choice of boundary conditions the auxiliary problem can be solved analytically, but we have to consider that the angular flux solution and/or its partial derivatives can be discontinuous across the singular characteristic (SC). The SC is given by all points for which $\bar{y} = \left|\frac{\eta_n}{\mu_n}\right| \bar{x}$ holds true where $\bar{x}$ and $\bar{y}$ are defined as

$$\begin{aligned} \bar{x} &= \frac{1 - \text{sign}(\mu_n)}{2} X + \text{sign}(\mu_n) x \\ \bar{y} &= \frac{1 - \text{sign}(\eta_n)}{2} Y + \text{sign}(\eta_n) y. \end{aligned} \tag{6}$$

It is the line of demarkation between regions illuminated by the left(L) for $\mu_n > 0$ or right edge(R) for $\mu_n < 0$ and the bottom(B) for $\eta_n > 0$ or top(T) edge for $\eta_n < 0$, see Fig. 1. Using the above definitions the solution of the auxiliary problem can be written as:

$$\psi_n(x,y) = \begin{cases} \psi_{<B,T>,n}\left(x - \text{sign}(\mu_n)\left|\frac{\mu_n}{\eta_n}\right|\bar{y}\right) e^{-\frac{\sigma_t}{|\eta_n|}\bar{y}} + \frac{Q}{\sigma_t}\left(1 - e^{-\frac{\sigma_t}{|\eta_n|}\bar{y}}\right) & \text{if } \bar{y} < \left|\frac{\eta_n}{\mu_n}\right|\bar{x} \\ \psi_{<L,R>,n}\left(y - \text{sign}(\eta_n)\left|\frac{\eta_n}{\mu_n}\right|\bar{x}\right) e^{-\frac{\sigma_t}{|\mu_n|}\bar{x}} + \frac{Q}{\sigma_t}\left(1 - e^{-\frac{\sigma_t}{|\mu_n|}\bar{x}}\right) & \text{if } \bar{y} > \left|\frac{\eta_n}{\mu_n}\right|\bar{x} \end{cases}. \quad (7)$$

The first term in each solution stencil represents the flux contribution from the boundary conditions, while the second term corresponds to the flux contribution from the distributed source. In the above equation we denote by $\psi_{<B,T>,n}(x)$ and $\psi_{<L,R>,n}(y)$ the boundary condition along the bottom or top edge and the left or right edge, respectively. Finally, we need to determine the

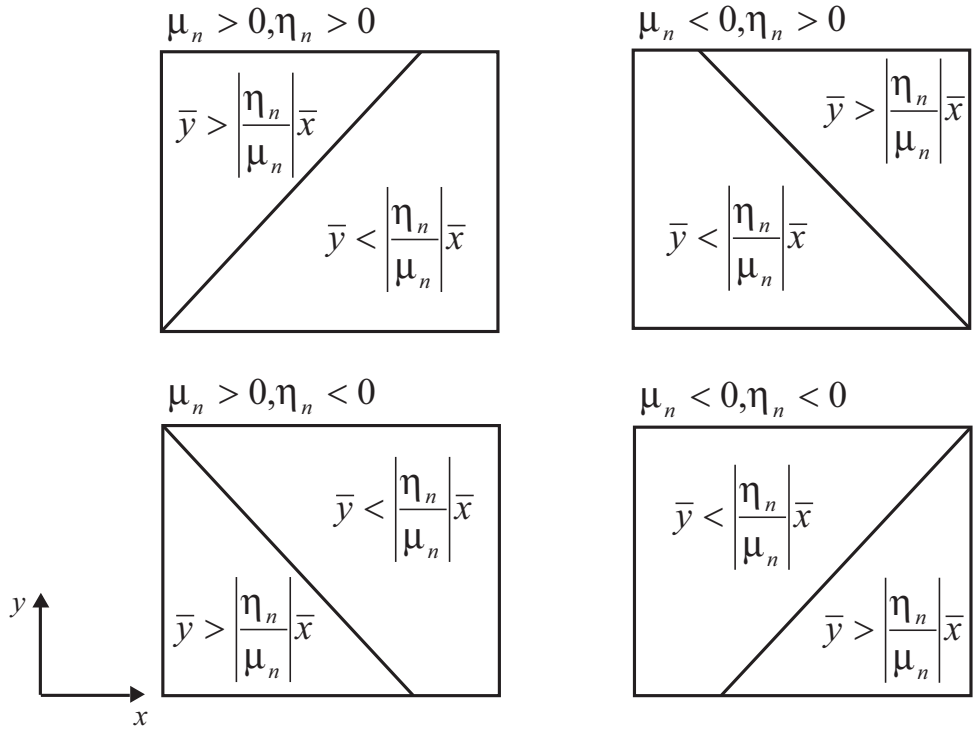


**Figure 1: Illustration of the singular characteristic and the resulting two solution stencils above and below the singular characteristic for all combinations of signs of $\mu_n$ and $\eta_n$.**

source $q(x,y)$ such that Eq. 7 is a manufactured solution for the model problem given by Eqs. 1 through 3. To this end we first note that since the model and auxiliary problem feature the same boundary conditions, the manufactured solution automatically satisfies Eq. 2. Further, we note that the manufactured solution satisfies Eq. 5, which upon substitution into Eq. 4 gives:

$$q(x,y) = Q - \sigma_s \phi(x,y). \quad (8)$$

In summary, Eq. 7 is a solution of the model problem given by Eqs. 1 and 2 if the distributed source is chosen according to Eq. 8 and the scalar flux is computed by substituting the manufactured solution Eq. 7 into Eq. 3. The whole procedure amounts to computing the uncollided flux given an auxiliary source $Q$ and then adjusting the source term to account for scattering.

**Table I: Example of parameters satisfying smoothness and positivity restrictions.**

| Smoothness | Smoothness Condition | Boundary Condition | Positivity Constraint |
|---|---|---|---|
| C0 | $[[\psi_n]]_{SC} \neq 0$ | $\psi_{<L,R>,n} = a_L \neq 0$<br>$\psi_{<B,T>,n} = 0$ | $\frac{Q}{\sigma_t} \leq a_L \leq \frac{Q}{\sigma_s\left(N \max\limits_n w_n\right)}$ |
| C1 | $[[\psi_n]]_{SC} = 0$<br>$\left[\left[\frac{\partial \psi_n}{\partial x}\right]\right]_{SC} \neq 0$ | $\psi_{<L,R>,n} = 0$<br>$\psi_{<B,T>,n} = 0$ | $\frac{\sigma_s}{\sigma_t}\left(N \max\limits_n w_n\right) \leq 1$ |
| Cp p $\geq 2$ | $[[\mathcal{H}_{p-1}]]_{SC} = 0$<br>$\left[\left[\frac{\partial^p \psi_n}{\partial x^p}\right]\right]_{SC} \neq 0$ | $\psi_{<L,R>,n} = \frac{Q}{\sigma_t} + a_p \bar{y}^p$<br>$\psi_{<B,T>,n} = \frac{Q}{\sigma_t} + a_p \bar{x}^p$ | $a_p \leq \frac{Q\left(1-\frac{\sigma_s}{\sigma_t}\left(N \max\limits_n w_n\right)\right)}{\sigma_s \max(X^p, Y^p)\left(N \max\limits_n w_n\right)}$ |

### 2.1 Order of Smoothness of the MMS

As mentioned above one of the key aspects of the described MMS benchmark suite is to allow for an arbitrary smoothness of the manufactured solution across the singular characteristic. It is possible to attain any desired smoothness by appropriately choosing the auxiliary source $Q$ and polynomial boundary conditions, i.e. the boundary conditions have the general functional form

$$\psi_{BC,n}(z) = \sum_{i=0}^{I} a_i z^i \tag{9}$$

along an incoming edge. For a formal treatment of the discontinuities it is useful to introduce the jump operator across the singular characteristic for a tensor of order $d$ of functions $f_{k_1,...,k_d}(x,y)$ indexed by $k_1,...,k_d$ defined on $\mathcal{D}$ featuring two separate solution stencils above, $f^{(a)}_{k_1,...,k_d}$, and below, $f^{(b)}_{k_1,...,k_d}$, the SC:

$$[[f_{k_1,...,k_d}(x,y)]]_{SC} = \left(f^{(a)}_{k_1,...,k_d}\left(\bar{x}, \left|\frac{\eta_n}{\mu_n}\right| \bar{x}\right) - f^{(b)}_{k_1,...,k_d}\left(\bar{x}, \left|\frac{\eta_n}{\mu_n}\right| \bar{x}\right)\right). \tag{10}$$

Let the order of any partial derivative, denoted by $\alpha_n$, be the sum of the orders of derivatives with respect to $x$ and $y$, i.e. $\alpha_n = \alpha_{n,x} + \alpha_{n,y}$. Further, we refer to the order of smoothness C$p$ of the DO solution $\psi_n$ for $n = 1,..,N$ as the lowest order partial derivative that is not continuous across the SC, i.e.:

$$p = \min_{n\in[1,N]} \alpha_n \text{ s.t. } \left[\left[\frac{\partial^{\alpha_{n,x}}\partial^{\alpha_{n,y}}\psi_n}{\partial x^{\alpha_{n,x}}\partial y^{\alpha_{n,y}}}\right]\right]_{SC} \neq 0 \tag{11}$$

Conditions on the boundary conditions and $Q$ can be derived for any desired order of smoothness by requiring that partial derivatives up to a certain order are continuous but at least one higher order partial derivative is not, e.g. for $C2$ continuity we require the gradient to be continuous while one second order derivative must be discontinuous. The imposed conditions and resulting non-unique set of boundary conditions are given in Table I, where $\mathcal{H}_p$ is the $p$th order tensor that collects all partial derivatives up to order $p$ (gradient, Hessian and so forth).

### 2.2 Positivity of the Distributed Source

The distributed source of the model problem $q(x,y)$ is calculated as the difference between the auxiliary source and the scattering source. For a sufficiently large scattering source this expression can become negative for some $x,y \in \mathcal{D}$ which is undesireable for two reasons. First, the physical meaning of the source does not allow for negative values[1] and second negative source values can pose a problem for subsequent usage in codes some of which might not allow negative sources. Hence, it is desireable to restrict the choice of the free parameters, i.e. $Q$ and the boundary conditions, to values that ensure a positive source $q$. It should be stressed here that the data that the MMS benchmark suite provides for subsequent usage are spatial moments of the flux and source within each mesh cells and hence, in practice, positivity contraints only extend to spatial averages of the source. The constraints we impose are a sufficient but not a necessary condition for the mesh cell averaged source to be positive. Note, however, if we allowed the model source to be negative for some $x$ and $y$, then for a sufficiently fine mesh some cell averaged source will be negative since mesh refinement localizes the occuring negative patches. In order to facilitate refinement studies on fine spatial meshes, we opt to impose the constraint that the source $q(x,y)$ is greater or equal to zero pointwise which leads to:

$$q(x,y) = Q - \sigma_s \sum_{n=1}^{N} w_n \psi_n(x,y) \geq Q - \sigma_s \left( N \max_n w_n \right) \max_{n,x,y} \psi_n(x,y) \geq 0. \tag{12}$$

The quadrature and thus the weights $w_n$ must be identical to the ones used in the code of interest and are hence predetermined; hence it only remains to determine the maximum of the angular flux $\max_{n,x,y} \psi_n(x,y)$ from Eq. 7. The restrictions arising from this analysis are presented in Table I for the set of boundary conditions that were chosen to attain the desired levels of smoothness.

## 3. IMPLEMENTATION OF THE MMS BENCHMARK SUITE IN MSBS-2D

The MMS benchmark suite implemented in the computer code MSBS-2D (Manufactured Solution Benchmark Suite in 2D) is aimed at providing reference solutions for any variation of Larsen's benchmark featuring polynomial boundary conditions independent of the angular variable. The domain size, the Cartesian mesh, cross sections, auxiliary source and boundary conditions are set by the user; the aforementioned constraints are not enforced by MSBS-2D although a warning is issued if a negative source cell-average occurs. The preceding section might be used as guidance by the user for finding a suitable choice of input parameters. The output of MSBS-2D comprises spatial Legendre Polynomial moments up to arbitrary order of the model source, boundary condition, the angular flux and the scalar flux. To summarize the function of MSBS-2D: It first tracks which mesh cells are intersected by the SC and divides these cells into two stencils each of which is further subdivided into triangles. Subsequently, the angular flux Eq. 7 is integrated analytically over the rectangular mesh cells and triangular subdivisions of mesh cells providing the angular flux moments and scalar flux moments are incremented on the fly using Eq. 3. Finally Eq. 8 is used to compute the source $q$. A brief description of the employed algorithms for the tracking and analytical integration follows.

[1] For verification purposes this is not a concern since verification is a purely mathematical exercise.

**Algorithm 1** SC Tracking

Set $i = \frac{1-sign(\mu_n)}{2} I$ and $j = \frac{1-sign(\eta_n)}{2} J$ and $\vec{x}_{out} = (x_i, y_j)$
**while** $1 \leq i \leq I$ and $1 \leq j \leq J$ **do**
  $\vec{x}_{in} = \vec{x}_{out}$
  **if** $|x_{i+\Delta i}\kappa_n + c_n - y_{j+\Delta j}| < 3\,|\kappa_n| \max(X, Y)\, \epsilon_{mach}$ **then**
    Intersection with corner.
    $i := i + \Delta i$, $j := j + \Delta j$, $\vec{x}_{out} := (x_i, y_j)^T$.
  **else**
    **if** $\eta_n (x_{i+\Delta i}\kappa_n + c_n) < \eta_n y_{j+\Delta j}$ **then**
      Intersection with left or right edge.
      $i := i + \Delta i$, $\vec{x}_{out} := (x_i, \kappa_n x_i + c_n)^T$.
    **else if** $\mu_n \frac{y_{j+\Delta j} - c_n}{\kappa_n} < \mu_n x_{i+\Delta i}$ **then**
      Intersection with bottom or top edge.
      $j := j + \Delta j$, $\vec{x}_{out} := (\frac{y_j - c_n}{\kappa_n}, y_j)^T$.
    **else**
      STOP. Print Error.
    **end if**
  **end if**
  Add cell intersection to linked list.
**end while**

### 3.1 Tracking Algorithm

Let the SC for DO $n$ be given by all points that satisfy $y = \kappa_n x + c_n$ with:

$$\kappa_n = \frac{\eta_n}{\mu_n}$$

$$c_n = \frac{1 - \text{sign}(\eta_n)}{2} Y - \kappa_n \frac{1 - \text{sign}(\mu_n)}{2} X. \tag{13}$$

Further, let $\Delta i = \text{sign}(\mu_n)$ and $\Delta j = \text{sign}(\eta_n)$ be increments of the $x$ and $y$ cell indices and $x_i$ and $y_j$ be cell boundaries where $i = 0, .., I$ and $j = 0, .., I$. Further the vector $\vec{x}$ is composed of the two components $\vec{x} = (x, y)^T$. The tracking algorithm Alg. 1 is based on the idea of following the SC along its path from the corner it originates from to the point where it leaves the domain. Within each mesh cell, the edge (or corner) through which the SC leaves is determined and $i$ and $j$ are incremented accordingly. It should be stressed that testing the intersection of the SC with a mesh cell corner has to explicitly take into account the finite precision arithmetic. In the framework of the tracking algorithm a tolerance is defined as the product of $\epsilon_{mach}$, the smallest normalized double precision number, and the maximum value that the left hand side of the intersection condition can possibly attain. Instead of requiring the intersection condition to be exactly zero, it is required to be smaller than the tolerance for a corner intersection to occur. The cells that are intersected by the SC are finally stored in a linked list since their total number is unknown prior to sweeping the full distance along the SC and hence a preallocated array cannot be used. Although the moderate number of spatial cells in two-dimensional meshes would allow for a brute force calculation of the intersection of the SC with the edges of all cells, the ultimate goal of this research is to implement a three-dimensional MMS benchmark suite, where such an approach is likely to be prohibitively expensive.

### 3.2 Analytical Integration Algorithm

One of the extraordinary features of the presented MMS benchmark suite is the fact that integrations are carried out anlytically as opposed to common practice in the field as e.g. in [10] to evaluate integrations using quadrature rules. Although employing a quadrature rule simplifies the implementation of the benchmark suite, it introduces the truncation error of the numerical integration as another source of error into the computation of the reference solution. For the sake of quality assurance of the manufactured solution it is then necessary to provide a reliable upper bound of the truncation error which relativizes the advantages gained by employing a quadrature rule. In contrast, an analytical evaluation can potentially only suffer from finite precision arithmetic errors. In general the output for subsequent use are spatial Legendre moments of the angular and scalar flux and the source $q$. As the source and scalar flux moments can be easily computed from the angular flux moments, it is sufficient to discuss the computation of the angular flux moment of order $l$, $m$ given by:

$$\psi_n^{(l,m)} = \frac{1}{\Delta x \Delta y} \int_{\Delta x} \int_{\Delta y} dxdy \; P_l\left(2\frac{x-x_c}{\Delta x}\right) P_m\left(2\frac{y-y_c}{\Delta y}\right) \psi_n(x,y), \tag{14}$$

where $(x_c, y_c)^T$ is the cell midpoint, $\Delta x$ and $\Delta y$ is the extent of the cell in $x$ and $y$ direction and $P_k(z)$ is the Legendre Polynomial of order $k$ normlized as in [11].

#### 3.2.1 Integration over Rectangular Cells

For the demonstration of the analytical integration over rectangular mesh cells assume that the considered DO is in the first angular quadrant and the cell is illuminated by the bottom edge, then we substitute Eqs. 7 and 9 into Eq. 14 to obtain:

$$\psi_n^{(l,m)} = \frac{1}{\Delta x \Delta y} \int_{\Delta x} \int_{\Delta y} dxdy P_l\left(2\frac{x-x_c}{\Delta x}\right) P_m\left(2\frac{y-y_c}{\Delta y}\right) \left\{ \left[\sum_{i=0}^{I} a_i \left(x - \frac{\mu_n}{\eta_n} y\right)^i\right] e^{-\frac{\sigma_t}{\eta_n} y} + \frac{Q}{\sigma_t}\left(1 - e^{-\frac{\sigma_t}{\eta_n} y}\right)\right\}. \tag{15}$$

The Legendre Polynomials are then expressed as sums of monomials:

$$\psi_n^{(l,m)} = \frac{1}{\Delta x \Delta y} \int_{\Delta x} \int_{\Delta y} dxdy \left\{\sum_{i=0}^{l} p_i \left(2\frac{x-x_c}{\Delta x}\right)^i\right\} \left\{\sum_{i=0}^{m} p_i \left(2\frac{y-y_c}{\Delta y}\right)^i\right\}$$
$$\times \left\{ \left[\sum_{i=0}^{I} a_i \left(x - \frac{\mu_n}{\eta_n} y\right)^i\right] e^{-\frac{\sigma_t}{\eta_n} y} + \frac{Q}{\sigma_t}\left(1 - e^{-\frac{\sigma_t}{\eta_n} y}\right)\right\}. \tag{16}$$

Then the three polynomials are multiplied out and the resulting sum is ordered by powers of $x$ and $y$:

$$\psi_n^{(l,m)} = \frac{1}{\Delta x \Delta y} \left\{ \sum_{i=0}^{l+I} \sum_{j=0}^{m+I} c_{i,j} \left[\int_{\Delta x} dx x^i\right] \left[\int_{\Delta y} dy y^j e^{-\frac{\sigma_t}{\eta_n} y}\right] \right\}, \tag{17}$$

where the coefficient of the double summation $c_{i,j}$ follows directly from multiplying out the various sums. We have implemented a framework of polynomial arithmetic routines that perform all necessary computations in Eq. 17 without approximation. The above equation is now amenable to standard integration formulas.

### 3.2.2 Integration over Triangular Subcells

The computation of the spatial flux moments for cells that are intersected by the SC proceeds in two steps. First, the total contributions $\delta\psi_{n,r}^{(l,m)}$ of all the subdomains $r = 1, .., R$ to the integral in Eq. 14 are computed and added up, then the sum is normalized by the area of the mesh cell:

$$\psi_n^{(l,m)} = \frac{\sum_{r=1}^{R} \delta\psi_{n,r}^{(l,m)}}{\Delta x \Delta y}. \tag{18}$$

Conveniently, a transformation of variables $\vec{x} = (x, y)^T \rightarrow \vec{u} = (u, v)^T$ is applied mapping the original triangle onto the unit triangle $u + v \leq 1$, $u, v \geq 0$:

$$\begin{aligned} x &= J_{1,1}u + J_{1,2}v + b_1 \\ y &= J_{2,1}u + J_{2,2}v + b_2, \end{aligned} \tag{19}$$

where $J_{i,j}$ is an entry of the transformation Jacobian $J$. Then for an arbitrary triangular subregion illuminated by the bottom boundary and DO in the first angular quadrant $\delta\psi_{n,r}^{(l,m)}$ can be expressed as:

$$\begin{aligned} \delta\psi_{n,r}^{(n,m)} = |J| \int_0^1 du \int_0^{1-u} dv \left\{ \sum_{i=0}^{l} p_i \left( 2\frac{J_{1,1}u + J_{1,2}v + b_1 - x_c}{\Delta x} \right)^i \right\} \left\{ \sum_{i=0}^{m} p_i \left( 2\frac{J_{2,1}u + J_{2,2}v + b_2 - y_c}{\Delta y} \right)^i \right\} \\ \times \left\{ \left[ \sum_{i=0}^{I} a_i \left( \left( J_{1,1} - \frac{\mu_n}{\eta_n} J_{2,1} \right) u + \left( J_{1,2} - \frac{\mu_n}{\eta_n} J_{2,2} \right) v + b_1 + b_2 \right)^i \right] e^{-\frac{\sigma_t}{\eta_n}(J_{2,1}u + J_{2,2}v + b_2)} \right. \\ \left. + \frac{Q}{\sigma_t} \left( 1 - e^{-\frac{\sigma_t}{\eta_n}(J_{2,1}u + J_{2,2}v + b_2)} \right) \right\}. \end{aligned} \tag{20}$$

Analogous to the integration over the rectangular mesh cells, the various sums are multiplied out and a double summation over powers of $u$ and $v$ can be obtained:

$$\delta\psi_{n,r}^{(n,m)} = |J|\, e^{\gamma} \sum_{i=0}^{n+m+I} \sum_{i=0}^{n+m+I} c_{i,j} \int_0^1 du u^i e^{\alpha u} \int_0^{1-u} dv v^j e^{\beta v}, \tag{21}$$

where $c_{i,j}$, $\alpha$, $\beta$ and $\gamma$ are generic constants that follow directly from known data. The integral in the double summation can in general be evaluated using standard formulas from integration tables, but we opted to expand the exponential into a truncated Taylor series of order 19 whenever $|\alpha|, |\beta| < 2$, because numerical experiments showed a superior precision of the Taylor series expansion within that range. The presented approach to analytically integrating the angular flux moments across mesh cells suffers from two problems both related to separating the Legendre Polynomials into its summands. First, the numerical precision deteriorates for higher order spatial moments, which has not been shown but is very likely to be caused by not treating the Legendre polynomials as unseparable functions [12]. In order to address this problem, all analytical integrations and the polynomial arithmetic are carried out in quadruple (128-bit) precision. Second, as the desired spatial order is increased nested loops several levels deep have to be evaluated causing the execution time to grow very quickly for higher spatial moments. In conjunction with the execution time penalty originating from the increased precision the MMS benchmark suite is bound to execute very slowly in certain cases. We believe that an implementation based on recursion, if found to be numerically stable, would alleviate both of these problems.

**Table II: Parameters for test cases I-III used for the error estimation examples.**

| Test Case | Cp | $\sigma_t$ | $c = \frac{\sigma_s}{\sigma_t}$ | X | Y | $\psi_{<B,T>,n}$ | $\psi_{<L,R>,n}$ | Q |
|---|---|---|---|---|---|---|---|---|
| Test Case I | C0 | 1.0 | 0.2 | 1.0 | 1.0 | 0 | 5 | 1 |
| | C1 | 1.0 | 0.2 | 1.0 | 1.0 | 0 | 0 | 1 |
| Test Case II | C0 | 10.0 | 0.2 | 1.0 | 1.0 | 0 | 5 | 10 |
| | C1 | 10.0 | 0.2 | 1.0 | 1.0 | 0 | 0 | 10 |
| Test Case III | C0 | 1.0 | 0.2 | 1.3 | 0.9 | 0 | 5 | 1 |
| | C1 | 1.0 | 0.2 | 1.3 | 0.9 | 0 | 0 | 1 |

## 4. NUMERICAL EXAMPLES

The numerical examples reported below illustrate the two areas of application targeted in this work, error estimation and computer code verification. In both cases test problems generated with the MMS benchmark suite are solved on a series of meshes featuring $2^k \times 2^k$ mesh cells with $k = 0, 1, .., 12$ and the accuracy of each solution is measured using a discrete version of an $L_2$ norm given by:

$$\|\epsilon\|_2 = \sqrt{\sum_{n=1}^{N} w_n \sum_{i=1}^{k}\sum_{j=1}^{k} A_{i,j}\left(\bar{\psi}_{n,i,j} - \bar{\psi}^{ref}_{n,i,j}\right)^2}. \tag{22}$$

In Eq. 22 $i$ and $j$ are the cell indices in $x$ and $y$ directions, respectively, $A_{i,j}$ is the area of cell $i, j$ and $\bar{\psi}_{n,i,j} = \psi^{(0,0)}_{n,i,j}$. All examples employ the $S4$ level symmetric quadrature.

### 4.1 Error Estimation

We used MSBS-2D to generate 3 test cases with specifications given in Table II. The example presented here only employs test cases with a differentiability of C0 and C1, since problems found in reality never exceed a smoothness of C1. Then C0 is most akin to a shielding application with shadowing and C1 represents e.g. a reactor physics application. In the framework of the example two spatial discretization schemes are compared: The arbitrarily high order nodal method (AHOTN) described e.g. in [11] and the higher-order Diamond Difference method (HODD) as introduced in [13]. The $L_2$ error for spatial orders $\Lambda = 0, 1, 2$ for test cases I and II and spatial orders $\Lambda = 0, 1$ for test case III are plotted vs. the number of degrees of freedom(DoF) in Figs. 2 through 4. We thereby denote by AHOTN$\Lambda$ and HODD$\Lambda$ the respective scheme of spatial expansion order $\Lambda$. For all three test cases we observe that HODD is asymptotically equivalent to AHOTN, i.e. in the limit of infinitely fine cells the two schemes are equivalent. This has been widely known for AHOTN0 and HODD0 (Diamond Difference) [8], but has to our knowledges not been asserted for higher spatial expansion orders. Further, AHOTN yields a better accuracy outside of the asymptotic regime which is most pronounced for optically thick domains, a smoothness of C0 and a spatial order of $\Lambda = 0$ (see Fig. 3). It should be mentioned

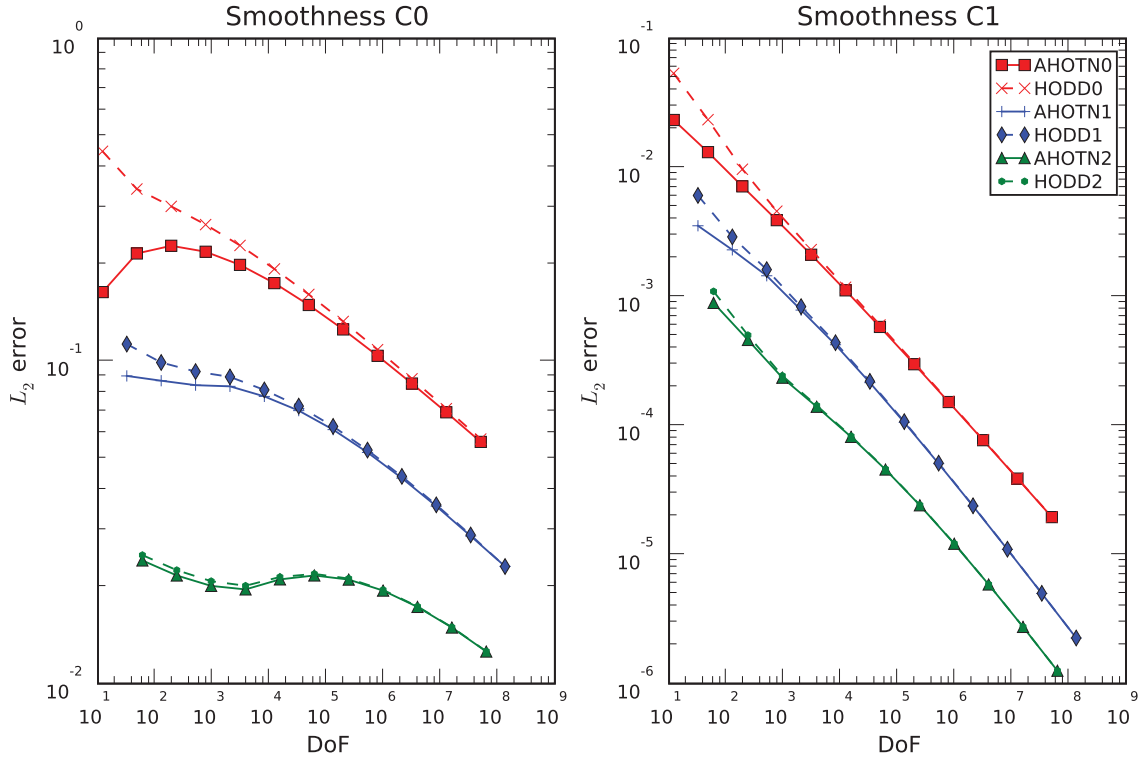


**Figure 2: $L_2$ errors vs. degrees of freedom (DoF) for AHOTN and HODD for test case I.**

that some of the error curves in Figs. 2 through 4 exhibit a maximum. The occurence of a maximum can be attributed to cancellation of errors across coarse mesh cells due to a lack of resolution close to the boundary and is a direct consequence of using the discrete error norm Eq. 22. For optically thin domains as e.g. in Fig. 2 and especially for the C1 cases, AHOTN is only marginally more accurate than HODD. To what extent the gain in accuracy outweighs the potential increase in execution time due to the evaluation of the spatial weights [11], has not been investigated in the presented research yet, but is subject to current research. Finally, the domain's shape (square in Fig. 2 and rectangular in Fig. 4) does not seem to have any influence on the performance of the two schemes, as the results are not altered by changing the domain shape and size.

### 4.2 Computer Code Verification

In contrast to error estimation, computer code verification employs test cases that are smooth enough such that the discretization scheme of interest can achieve its maximum rate of convergence $r$ defined as:

$$r = \frac{log\left(\frac{\|\epsilon\|_{2,k}}{\|\epsilon\|_{2,k-1}}\right)}{log(2)} \tag{23}$$

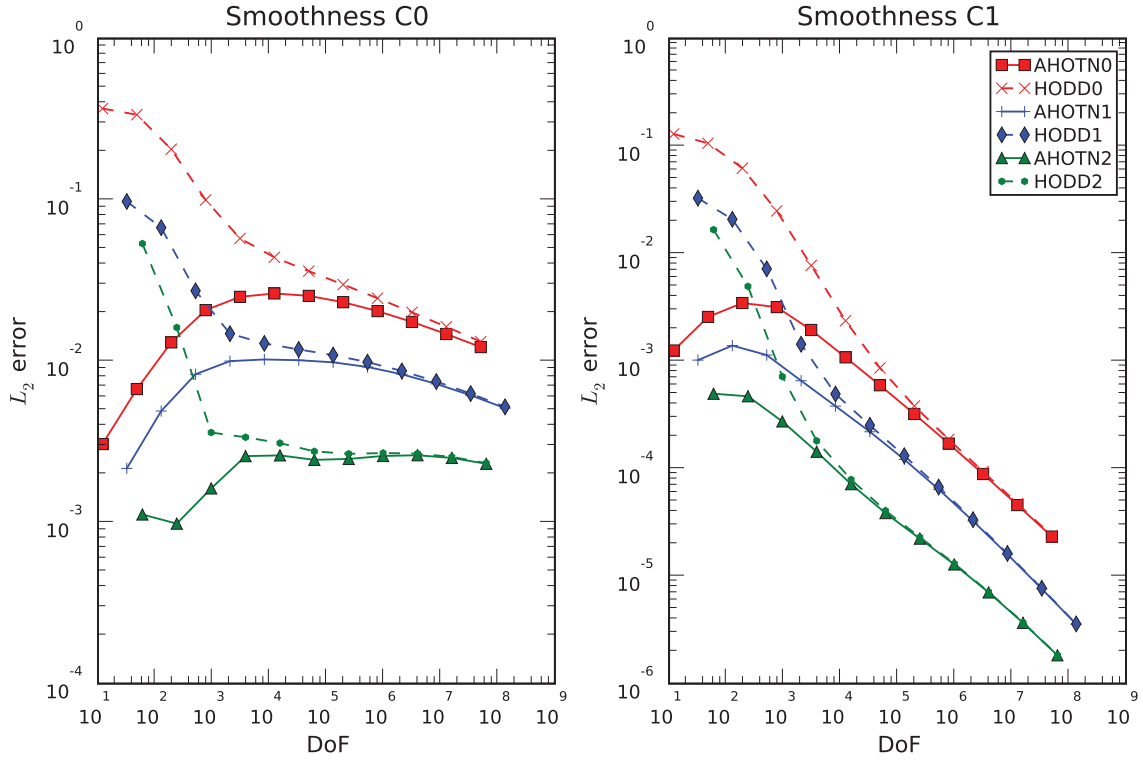


**Figure 3: $L_2$ errors vs. degrees of freedom (DoF) for AHOTN and HODD for test case II.**

For demonstrating how the MMS benchmark suite can be used for computer code verification we set up test cases with smoothness C0, C2, C4 and C6 and perform grid refinement studies employing AHOTN0 and AHOTN1 implementations. We use the cross sections and geometrical specifications of test case I and boundary conditions and auxiliary source given in Table III for the various degrees of smoothness. The maximum rate of convergence of AHOTN$\Lambda$ is $r_{max} = 2\Lambda + 2$ if the exact solution possesses a sufficient number of bounded partial derivatives such that for $\Lambda = 0$ we expect $r_{max} = 2$ and for $\Lambda = 1$ we expect $r_{max} = 4$ [5]. The $L_2$ error vs. degrees of freedom is plotted in Fig. 5 and the asymptotic rates of convergence $r$ are presented in Table IV. For C0 and C2 the smoothness of the underlying exact solution controls the rate of convergence since AHOTN0 and AHOTN1 converge almost at the same rate, in Fig. 5 the line indicating the first order scheme is just shifted to smaller errors but features the same slope. For C4 the slopes differ which is a consequence of the fact that AHOTN0 has already assumed its maximum rate of convergence(see Table IV), further increasing the smoothness of the underlying true solution will not affect the rate of convergence of AHOTN0. At this point we have verified the AHOTN0 implementation, but for AHOTN1 we do not obtain a 4th order rate of convergence. The first conclusion from this example is that the higher the spatial expansion order of the scheme of interest, the more bounded partial derivatives must exist in order to facilitate a convergence with the maximum possible order. Finally, for C6 the rate of convergence of both AHOTN0 and AHOTN1 has reached its maximum value $r_{max}$. Thus, both implementations are verified.

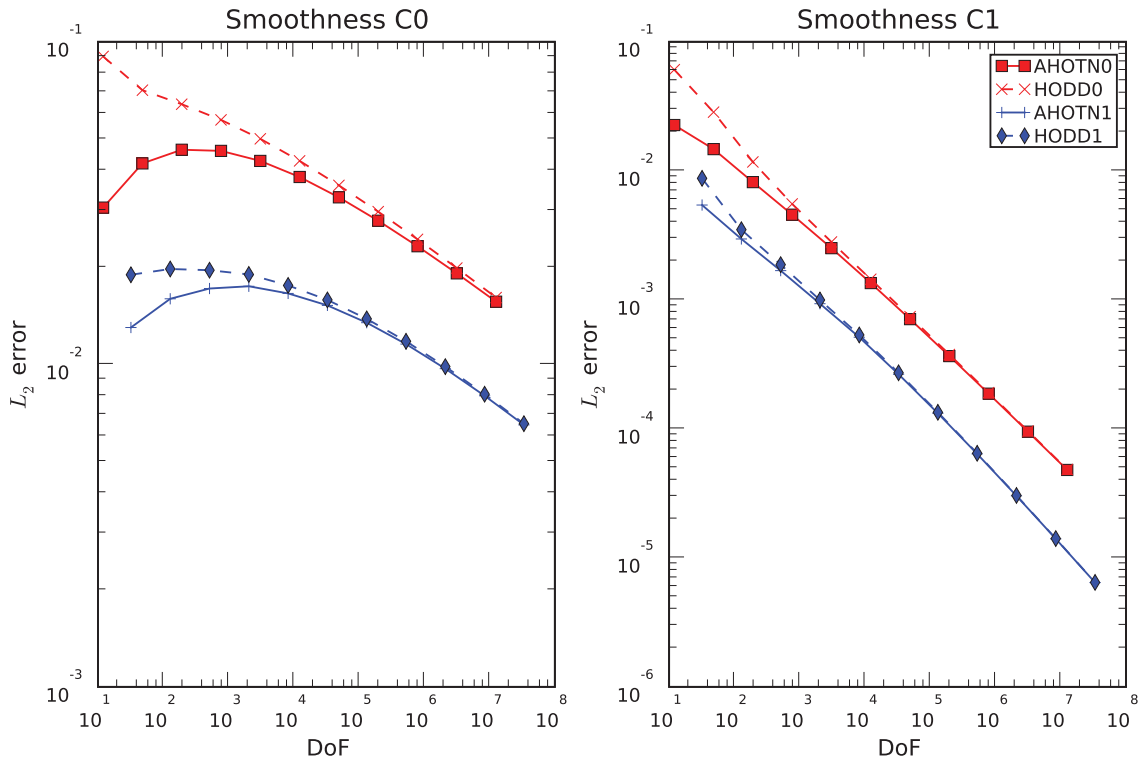


**Figure 4: $L_2$ errors vs. degrees of freedom (DoF) for AHOTN and HODD for test case III.**

**Table III: Choice of Boundary Conditions used in the verification study.**

| | Boundary Conditions | $Q$ |
|---|---|---|
| C0 | $\psi_{<B,T>} = 0$<br>$\psi_{<R,L>} = 5$ | 1 |
| C2 | $\psi_{<B,T>} = 1 + 4\bar{x}^2$<br>$\psi_{<R,L>} = 1 + 4\bar{y}^2$ | 1 |
| C4 | $\psi_{<B,T>} = 1 + 4\bar{x}^4$<br>$\psi_{<R,L>} = 1 + 4\bar{y}^4$ | 1 |
| C6 | $\psi_{<B,T>} = 1 + 4\bar{x}^6$<br>$\psi_{<R,L>} = 1 + 4\bar{y}^6$ | 1 |

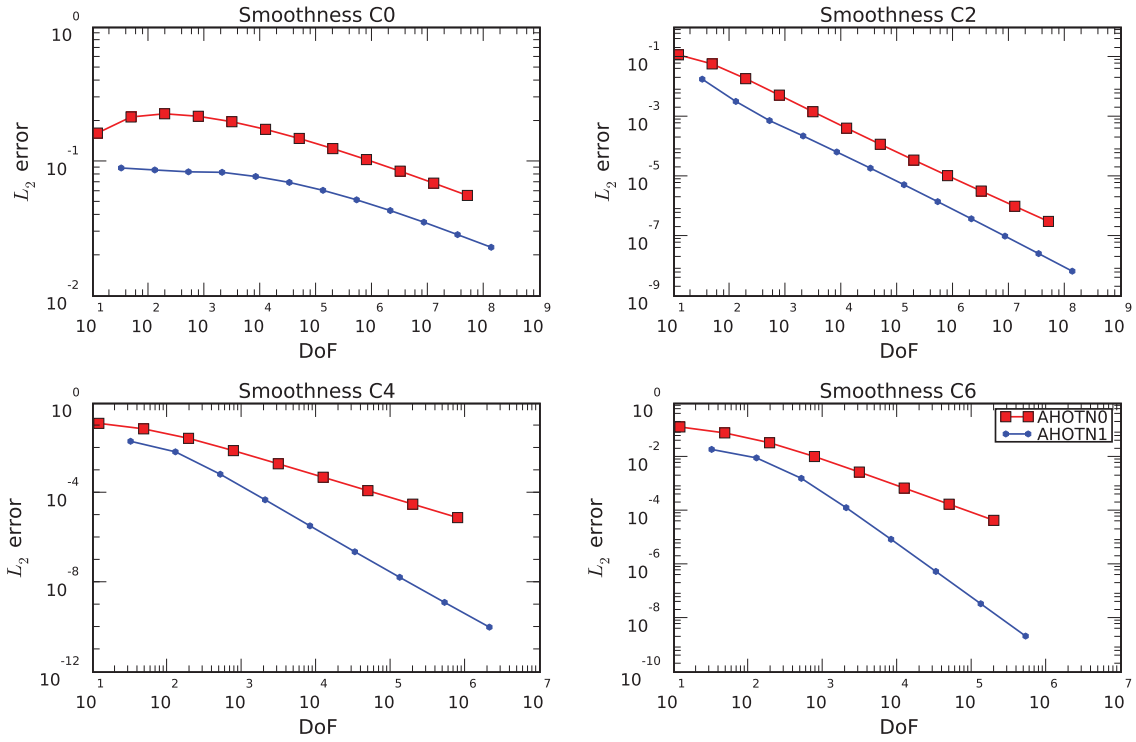


**Figure 5: $L_2$ errors vs. degrees of freedom (DoF) for AHOTN0 and AHOTN1 for various orders of smoothness.**

**Table IV: Rates of convergence of AHOTN0 and AHOTN1 for different orders of smoothness of the exact solution.**

| Scheme | C0 | C2 | C4 | C6 |
|---|---|---|---|---|
| AHOTN0 | 0.30 | 1.69 | 2.00 | 2.00 |
| AHOTN1 | 0.31 | 1.96 | 3.64 | 4.00 |

## 5. CONCLUSIONS

We presented a two-dimensional MMS benchmark suite for the DO equations on arbitrary Cartesian meshes based on Larsen's benchmark. The benchmark suite allows for an arbitrary degree of smoothness across the SC controlled by choices of the boundary conditions and auxiliary source, arbitrary material properties and Cartesian meshes. The code MSBS-2D that implements the MMS analytically computes spatial Legendre moments of the angular and scalar flux and the distributed source and writes them to file for subsequent use. Via the MMS benchmark suite we established that the AHOTN spatial discretization scheme performs better than the HODD

scheme if optically thick cells are used while both methods are asymptotically equivalent. Further, we verified the AHOTN implementations of order zero and one via test problems featuring an escalating order of smoothness by numerically reproducing the theoretically determined error orders. Both results illustrate the utility of the described MMS benchmark suite.

## REFERENCES


1. Larsen, E. W. and Miller, W.F. Jr. Convergence Rates of Spatial Difference Equations for the Discrete-Ordinated Neutron Transport Equations in Slab Geometry. *Nucl. Sci. Eng.*, **Vol. 73**, pp. 76-83 (1980).

2. Arkuszewski, J and Kulikowska, T and Mika, J. Effect of Singularities on Approximation in $S_N$ Methods. *Nucl. Sci. Eng.*, **Vol. 49**, pp. 20-26 (1972).

3. Warsa, James S. Analytical $S_N$ solutions in heterogeneous slabs using symbolic algebra computer programs. *Annals of Nuclear Energy*, **Vol. 29**, pp. 851-874 (2002).

4. Larsen, Edward W. and Nelson, Paul. Finite-Difference Approximation and Superconvergence for the Discrete-Ordinate Equations in Slab Geometry. *SIAM J. NUMER. ANAL.*, **Vol. 19**, pp. 334-348 (1982).

5. Victory, H.D. Jr. and Ganguly, Keshab. On Finite-Difference Methods for Solving Discrete Ordinates Transport Equations. *SIAM J. NUMER. ANAL.*, **Vol. 23**, pp. 78-108 (1986).

6. Wang, Yaqi and Ragusa Jean C. On the Convergence of DGFEM Applied to the Discrete Ordinates Transport Equation for Structured and Unstructured Triangular Meshes. *Nucl. Sci. Eng.*, **Vol. 163**, pp. 56-72 (2009).

7. Roy, C.J. Review of code and solution verification procedures for computational simulation. *J. Comp. Phys.*, **Vol. 205**, pp. 131 (2005).

8. Duo, Jose I. and Azmy, Yousry Y.Y. Spatial Convergence Study of Discrete Ordinates Methods Via the Singular Characteristic Tracking Algorithm. *Nucl. Sci. Eng.*, **Vol. 162**, pp. 41-55 (2009).

9. Larsen, E. W. Spatial Convergence Properties of the Diamond Difference Method in x,y Geometry *Nucl. Sci. Eng.*, **Vol. 80**, pp. 710 (1980).

10. Drumm, C. Order-Convergence Anomalies in Second-Order Finite Elements Transport Methods. *International Conference on Mathematics, Computational Methods & Reactor Physics.*, Saratoga Springs, May 3-7 2009 (2009).

11. Azmy, Y.Y. The Weighted Diamond-Difference Form of Nodal Transport Methods. *Nucl. Sci. Eng.*, **Vol. 98**, pp. 29 (1987).

12. Ganapol, B. Personal communication. Summer 2010.

13. Hebert, A. High Order Diamond Differencing Schemes. *Annals of Nuclear Energy*, **Vol. 33**, pp. 1479-1488 (2006).